Published in final edited form as:
Chembiochem. 2013 August 19; 14(12): . doi:10.1002/cbic.201300263.

Strand Invasion of DNA Quadruplexes by PNA: Comparison of Homologous and Complementary Hybridization

Anisha Gupta[a], **Ling-Ling Lee**[a], **Subhadeep Roy**[a], **Farial A. Tanious**[b], **W. David Wilson**[b], **Danith H. Ly**[a], and **Bruce A. Armitage**[a]

Bruce A. Armitage: army@cmu.edu

[a]Department of Chemistry and Center for Nucleic Acids Science and Technology, Carnegie Mellon University, 4400 Fifth Avenue, Pittsburgh, PA 15213

[b]Department of Chemistry, Georgia State University, Atlanta, GA 30303

Abstract

Molecular recognition of DNA quadruplex structures is envisioned as a strategy for regulating gene expression at the transcriptional level and for *in situ* analysis of telomere structure and function. The recognition of DNA quadruplexes by peptide nucleic acid (PNA) oligomers is presented here, with a focus on comparing complementary, heteroduplex-forming and homologous, heteroquadruplex-forming PNAs. Surface plasmon resonance and optical spectroscopy experiments demonstrated that the efficacy of a recognition mode depended strongly on the target. For a quadruplex derived from the promoter regulatory region found upstream of the *MYC* proto-oncogene, the homologous PNA readily invades the DNA target to form a heteroquadruplex at high potassium concentration mimicking the intracellular environment, whereas the complementary PNA exhibits virtually no hybridization. In contrast, the complementary PNA is superior to the homologous PNA in hybridizing to a quadruplex modeled on the human telomere sequence. The results are discussed in terms of the different structural morphologies of the quadruplex targets and the implications for *in vivo* recognition of quadruplexes by PNAs.

Introduction

The ability of DNA to adopt nonduplex secondary and tertiary structures has long been of fundamental and biological interest, but the discovery of quadruplex DNA is driving considerable new activity in this field.[1] Intramolecular quadruplex DNA forms from guanine-rich sequences that can fold back on themselves to allow hydrogen-bonded G-tetrad formation and pi-stacking mediated stabilization.[2] Quadruplex DNA is most stable in physiologically relevant concentrations of potassium, due to favorable coordination of the guanine O-6 atoms by potassium cations.[3] Bioinformatics studies showing the prevalence of quadruplex-forming sequence (QFS) motifs in the genome, particularly in promoter regions,[4] transcriptional reporter assays[5] and endogenous gene expression profiling[6] all point toward functional significance of quadruplex DNA.[7]

There are numerous reports of endogenous quadruplex-binding proteins.[8] These cofactors likely play important roles in stabilizing quadruplex secondary structures and recruiting other proteins involved in regulating gene expression. Artificial quadruplex-binding proteins have also been obtained through screening of diverse libraries and the resulting proteins have been used in a variety of experiments to identify quadruplex sites.[6, 9] A recent report

Correspondence to: Bruce A. Armitage, army@cmu.edu.

by Balasubramanian and coworkers illustrates the use of a quadruplex-binding protein as the primary recognition component in an immunofluorescence method for identifying chromosomal quadruplex motifs.[10]

A diverse collection of synthetic quadruplex-binding molecules has been reported over the past 20 years. These include small molecules obtained through traditional medicinal chemistry approaches, which are expected to recognize quadruplexes through binding to specific three-dimensional structural motifs.[11] The most notable of these molecules feature sub-micromolar affinities and demonstrate significant intracellular activity against suspected quadruplex targets.

An alternative approach to recognizing quadruplexes relies on specific hydrogen bonding to the nucleobases by oligomeric compounds. The most straightforward design involves Watson-Crick recognition, i.e. a cytosine-rich oligomer that can bind in a complementary fashion to a G-rich target. The majority of reports describing this approach have involved C-rich peptide nucleic acids (PNAs).[12] Typically, binding of the complementary PNA competes with quadruplex formation,[13] although a recent report from Mayol and coworkers describes the binding of short PNAs to accessible loops without disruption of the underlying quadruplex secondary structure.[14]

Quadruplexes can also be recognized by G-rich PNAs, in which case the resulting hybrids are heteroquadruplexes, rather than heteroduplexes.[15] A variety of quadruplex structures and stoichiometries can be obtained in this manner. For example, targeting a folded DNA quadruplex with a PNA having two G_3 tracts results in formation of a PNA_2-DNA complex consisting of two PNA-DNA heteroquadruplexes linked via a short DNA tether that was originally a loop in the DNA homoquadruplex target.[16] Alternatively, a PNA having a single G_3 tract can hybridize to a DNA having three G_3 tracts to form a 1:1 heteroquadruplex.[17]

While targeting quadruplexes with either C-rich complementary or G-rich homologous PNA appears to involve sequence-based recognition as opposed to the structure-based recognition commonly associated with small molecules, we recently discovered that a quadruplex-forming PNA exhibited more than 10-fold difference in association kinetics within a group of morphologically diverse DNA quadruplexes, indicating that the structure of the quadruplex can play an important role in PNA heteroquadruplex formation, at least from a kinetic perspective.[16a] This motivated our current studies to determine (a) if similar structural factors would be observed in the hybridization of complementary PNA to DNA quadruplexes and (b) if there are significant differences in the kinetics of hybridization between complementary and homologous PNAs for two DNA quadruplex targets.

Results

The overall goal of this work was to compare binding of homologous and complementary PNAs to DNA G-quadruplex targets. We started with a parallel quadruplex formed by a sequence modeled from the promoter region of the *MYC* proto-oncogene.[18] We previously demonstrated effective heteroquadruplex formation with this target by several G-rich PNAs with K_D values in the low nanomolar range.[16] One of those PNAs, which we previously referred to as P_{myc}, we now call $P_{myc}H$ to distinguish it from the complementary PNA, $P_{myc}C$ (Table 1). The homologous PNAs form 2:1 heteroquadruplexes with the DNA targets, so the complementary PNAs were designed to form 2:1 heteroduplexes. Also, note that PNA-DNA heteroduplex formation is known to favor alignment of the PNA N-terminus with the DNA 3′-terminus,[19] whereas the opposite orientational preference was found previously for a PNA-DNA heteroquadruplex.[15] Figure 1 illustrates our previously

proposed heteroquadruplex-binding model along with the expected 2:1 heteroduplex structure.

SPR Analysis of PNA Hybridization to the Myc19 Quadruplex

Surface plasmon resonance (SPR) experiments were previously helpful in studying heteroquadruplex formation at high ionic strength, where UV melting temperatures are too high to determine, allowing study of these nanomolar binding interactions from both kinetic and equilibrium perspectives.[16c] Therefore, we began this study by using SPR to compare hybridization of $P_{myc}H$ and $P_{myc}C$ to an immobilized Myc19 target. Figure 1A shows binding of the homologous PNA to the DNA target in the presence of 100 mM KCl, where the DNA should be folded into a stable quadruplex. We observe a concentration dependent increase in the binding of the PNA at relatively low nanomolar concentrations. As we observed previously, dissociation of the bound PNA is quite slow, reflecting formation of a stable heteroquadruplex. In contrast, when we performed the identical experiment with the complementary PNA $P_{myc}C$, negligible hybridization was observed (Figure 1B). This indicates that, under these conditions, formation of a PNA-DNA heteroduplex based on Watson-Crick base pairing is kinetically unfavorable, compared with PNA-DNA heteroquadruplex formation.

One possible explanation for the much slower hybridization of the complementary PNA is the stability of the Myc19 quadruplex structure in high potassium concentration. It is well known that replacing potassium by sodium reduces the stability of both DNA homoquadruplexes[3] and PNA-DNA heteroquadruplexes.[15, 16c] Therefore, we repeated the SPR experiments in sodium containing buffer (Figures 1C and 1D). There is relatively little change in the binding of $P_{myc}H$ to the target in NaCl versus KCl but $P_{myc}C$ now binds comparably to the homologous PNA. Changing the buffer to lithium further destabilizes the Myc19 quadruplex as well as the PNA-DNA heteroquadruplex but not the heteroduplex as shown by the results in Figures 1E and 1F, where $P_{myc}H$ shows much lower binding response whereas $P_{myc}C$ binding is further accelerated.

To more easily compare hybridization as a function of ion, Figure 2 shows SPR sensorgrams for a single PNA concentration (20 nM) in KCl, NaCl and LiCl. $P_{myc}H$ binds similarly in Na^+ versus K^+, indicating that the destabilizing effect of the change in ion is greater for the DNA homoquadruplex than for the PNA_2-DNA heteroquadruplex, allowing more PNA to hybridize during the association phase. In the presence of LiCl, the large drop in PNA binding during the association phase and the significantly faster dissociation are consistent with the overall quadruplex destabilizing effect of lithium. However, the opposite trend is observed for $P_{myc}C$; the complementary PNA clearly requires destabilization of the Myc19 quadruplex target in order to hybridize.

There is an additional interesting result evident from comparing the data obtained in different salts, particularly in Figures 1D and 1F: the binding signal is nearing saturation at ca. 150 response units in LiCl, whereas the signal in NaCl exceeds this value at the highest PNA concentration. We believe that weaker, higher-order complexes are forming at the higher PNA concentrations, based on the significantly faster dissociation rates evident in these sensorgrams compared with the lower PNA concentrations.

CD Analysis

Circular dichroism measurements are useful in the characterization of nucleic acid secondary structure and in the study of hybridization events. CD spectra were recorded for Myc19 DNA alone and in a 1:2 mixture with $P_{myc}C$ in 100 mM KCl buffer (Figure 3A). As, observed previously, Myc19 alone exhibits a negative peak at 240 nm and a positive peak at

265 nm, indicative of a parallel quadruplex.[20] Annealing $P_{myc}C$ with Myc19 yields a CD spectrum that is similar to that of Myc19 alone. This is consistent with the SPR data indicating minimal binding of the complementary PNA to the DNA quadruplex under these conditions. However, PNA-DNA heteroduplexes also exhibit CD maxima at 265 nm and minima at 240 nm,[19] hence, it is difficult at this point to infer whether the CD spectrum of the mixture is due to a heteroduplex or a homoquadruplex. In contrast, destabilizing the Myc19 quadruplex in NaCl or LiCl leads to more significant changes in the CD spectra upon addition of $P_{myc}C$ (Figures 3B and 3C). These results indicate that heteroduplex formation is favorable in sodium and lithium, consistent with the SPR results.

Cyanine Dye Binding to PNA-DNA Heteroduplexes

Further examination of heteroduplex formation was done using two cyanine dyes, $DiSC_2(5)$ and $DiSC_1(3)$. We previously demonstrated binding of $DiSC_2(5)$ to PNA-DNA heteroduplexes.[21] The dye binds by assembling into a helical aggregate using the PNA-DNA duplex as a template and is readily detected as a blue-purple color change as well as distinct visible absorption and induced CD bands. Figure 4 shows induced CD spectra for the dye in the presence of 1:2 Myc19:$P_{myc}C$. A very weak CD band is observed in the presence of KCl, with much higher intensity observed in NaCl and LiCl. Combined with the SPR and CD data described above, these results confirm that the complementary PNA binds very weakly to the Myc19 target in KCl solution. Moreover, the samples that were analyzed by CD in Figures 3 and 4 were annealed by heating to 90 °C followed by slow cooling to room temperature, giving the PNA ample opportunity to hybridize. Therefore, the poor binding evident in Figure 2B cannot be ascribed solely to a kinetic barrier to hybridization.

Based on the sequence of $P_{myc}C$, a 2:1 heteroduplex should form (Scheme 1). From the SPR, CD and UV results, we do not observe the formation of Myc19-$P_{myc}C$ duplex in 100 mM KCl so the binding stoichiometry was determined in 100 mM NaCl. We recently demonstrated the utility of another cyanine dye, $DiSC_1(3)$, in determining PNA-DNA binding stoichiometries, based on differences in fluorescence intensity for binding to DNA homoquadruplexes and PNA-containing hybrids.[22]

$DiSC_1(3)$ exhibits distinctive UV-vis and fluorescence spectra in the presence of the Myc19 homoquadruplex and Myc19-$P_{myc}C$ heteroduplex (Figure S1). These spectral differences are sufficient to allow a continuous variations experiment to be used to determine the binding stoichiometry. In this experiment, the dye concentration was held constant at 1 μM. The total DNA+PNA concentration was also held constant, but the ratio of the two oligomers was varied. Plotting the fluorescence intensity versus mole fraction of PNA results in an inflection at 0.67, i.e. a 1:2 DNA:PNA ratio (Figure 5). Thus, the complementary PNA is capable of binding to the Myc19 homoquadruplex in 1:2 stoichiometry, analogous to our previous findings for the homologous PNA, although only $P_{myc}H$ has sufficient affinity to do so in high potassium concentration.

PNA Hybridization to an Alternative Quadruplex Target

Overall, the results described above demonstrate both kinetic and thermodynamic advantages for targeting the Myc19 DNA quadruplex with heteroquadruplex-forming PNA over a comparable heteroduplex-forming PNA. However, we recently reported that the kinetics of PNA-DNA heteroquadruplex formation can vary over a wide range depending on the structure of the DNA quadruplex target.[16a] Therefore, we extended these studies to a DNA quadruplex that was more resistant kinetically to heteroquadruplex formation.

We used a DNA oligonucleotide, hTelo22 (Table 1), derived from the human telomeric repeat sequence $(GGGTTA)_{n.}$ DNA oligonucleotide models based on this sequence have

been shown to fold (in potassium solution) into a hybrid structure that features both parallel and antiparallel strand orientations.[23] In our previous work, homologous PNAs such as $P_{myc}H$ and $P_{telo}H$ exhibited more than 10-fold slower hybridization to hTelo22 than to Myc19. Thus, we were curious to see if the advantages described above for homologous PNA binding to Myc19 would be preserved for hTelo22.

Figure 6 provides SPR data for binding of $P_{telo}H$ and $P_{telo}C$ to the immobilized hTelo22 DNA target. In KCl, binding of $P_{telo}H$ to hTelo22 is much slower than the binding of $P_{myc}H$ to Myc19 (compare Figures 6A and 1A), consistent with our earlier findings. A similar experiment with the complementary PNA $P_{telo}C$ revealed significant hybridization even in the presence of KCl, in contrast to complementary hybridization to Myc19 (compare Figures 6B and 1B). Thus, in KCl solution, complementary PNA is better suited to binding to the telomeric quadruplex, whereas homologous PNA performs better with the Myc19 quadruplex.

We next repeated the SPR experiments in quadruplex-destabilizing sodium- or lithium-containing buffer. As shown in Figures 6C and 6E, $P_{telo}H$ binding to hTelo22 is only modestly improved in sodium and completely abolished in lithium, indicating that, while destabilization of the DNA quadruplex should accelerate heteroquadruplex formation, corresponding destabilization of the heteroquadruplex is also sufficiently high to minimize PNA hybridization. In contrast, hybridization of $P_{telo}C$ to hTelo22 increases significantly in the order KCl < NaCl < LiCl. Thus, complementary PNA hybridization to the two DNA quadruplexes follows a qualitatively similar cation dependence, although heteroduplex formation is noticeably better for hTelo22. In contrast, homologous PNA hybridization to the two quadruplexes is markedly better for Myc19, consistent with our previous findings.

Figure 7 overlays SPR sensorgrams for hybridization of the two PNAs to the hTelo22 quadruplex in the different salts. The significant advantage of the complementary PNA over the homologous PNA is evident for all three salts.

CD spectra were recorded for hTelo22 DNA alone and in a 1:2 mixture with $P_{telo}C$ in 100 mM KCl, NaCl or LiCl buffer (Figure 8). The CD spectrum for the quadruplex alone in KCl exhibits features associated with a hybrid structure, specifically a positive band at 295 nm and a shoulder at 260 nm. In the presence of the complementary PNA, the spectrum shifts to that expected for a PNA-DNA heteroduplex. Similar results upon addition of $P_{telo}C$ are observed in the other salts, consistent with the SPR results.

CD spectra and cyanine dye binding experiments confirmed the formation of a $P_{telo}C$:hTelo22 heteroduplex. As shown in Figure 9A, the induced CD signal from $DiSC_2(5)$ increased in the order KCl < NaCl < LiCl, consistent with increasing heteroduplex formation as the hTelo22 quadruplex is destabilized. The stronger CD signals compared with the Myc19 system (Figure 4) could reflect sequence preferences for $DiSC_2(5)$ binding to PNA-DNA duplexes, but this requires additional study to verify. In LiCl, the $P_{telo}C$:hTelo22 heteroduplex is formed in a 2:1 stoichiometry based on Job plot analysis using the fluorogenic cyanine $DiSC_1(3)$ (Figure 9B; absorbance and emission spectra shown in Figure S2).

DISCUSSION

Previous findings from our labs and others have shown that complementary and homologous PNA probes bind intramolecular RNA/DNA quadruplexes and form stable PNA-DNA heteroduplex or heteroquadruplex structures, respectively. In earlier studies, we compared the binding of homologous and complementary PNAs to an RNA aptamer, which had been selected for binding to the Fragile X mental retardation protein and adopts a G-quadruplex

structure.[24] There we found that that a 1:1 hybrid duplex and a 2:1 hybrid quadruplex were formed by complementary and homologous PNA probes respectively, but the complementary PNA was designed to target a central 7 nucleotide segment of the RNA, precluding 2:1 binding. In the current study, we specifically designed the complementary PNA to form a 2:1 complex to facilitate comparisons with the homologous PNA.

Myc19 Quadruplex

The Myc19 DNA quadruplex adopts a parallel morphology, with one-, two- and one-base loops formed as the strand folds back on itself in order to begin forming the next quadrant of the structure. The SPR results in Figure 1A and 1B illustrate the significant advantage possessed by the homologous PNA in invading the quadruplex structure in order to hybridize under high KCl conditions. The failure of the complementary PNA to bind under these conditions was also reflected in the CD results shown in Figures 3 and 4, indicating that even thermal annealing is insufficient to promote heteroduplex formation. (The consistency of these results also suggests that the parallel morphology of the Myc19 quadruplex is maintained whether in solution or immobilized on the SPR chip surface.) Thus, heteroquadruplex formation by the homologous PNA is both kinetically and thermodynamically favored over heteroduplex formation by the complementary PNA for this particular target. Only weakening of the DNA quadruplex by switching the cation to sodium or lithium allows the complementary PNA to bind to the Myc19 target. In contrast, Amato and coworkers reported that a short PNA hexamer (ACCCCA) was unable to invade a four-tetrad DNA quadruplex but could form stable heteroduplexes if thermally annealed with the target.[13c] The fluorogenic dye experiment shown in Figure 5 verifies that the complementary PNA forms a 2:1 heteroduplex, as designed.

hTelo22 Quadruplex

In contrast to the strong preference for heteroquadruplex versus heteroduplex recognition of Myc19 by PNA, SPR results shown in Figures 6 and 7 indicate that heteroduplex formation is favored for PNA recognition of hTelo22 under all ionic conditions and Figure 9B is consistent with a 2:1 stoichiometry for the heteroduplex.

It will be interesting to compare the results for telomeric DNA with telomeric RNA (TERRA), which (*i*) is transcribed using the C-rich strand as a template, (*ii*) is known to fold *in vitro* into a parallel quadruplex, and (*iii*) localizes to telomeric regions.[25] The results described here suggest that homologous recognition of TERRA by quadruplex-forming PNA should be much more efficient than recognition of the corresponding DNA due to the parallel structure of TERRA. However, the corresponding SPR experiments are difficult to perform with immobilized RNA due to the harsh (i.e. high pH) conditions needed to regenerate the chip after PNA hybridization. The reverse experiment, namely hybridization of DNA or RNA to immobilized PNA could be illuminating, although such experiments would preclude 2:1 PNA-DNA/RNA hybridization. Nevertheless, other kinetic methods such as monitoring fluorescence enhancement of a PNA-appended dye such as thiazole orange might be useful for comparing hybridization rates with different targets in solution.

The results described here illustrate significant differences between quadruplex-invading PNAs that form heteroduplexes versus heteroquadruplexes and how kinetic preferences depend strongly on the structure of the quadruplex target. Although there have been numerous reports describing the intracellular effects of quadruplex-binding small molecules, biological effects of quadruplex-targeting PNAs have yet to be investigated. Significantly, a recent report from Xu and coworkers describes the ability of quadruplex-forming short RNAs to down-regulate expression of an EGFP reporter gene in live cells.[26] The high affinity of PNA and recent advances in delivery of PNA into cells are expected to lead to

potent effects on gene expression.[27] It will be interesting to see if the differences reported here for complementary versus homologous PNA are reproduced in the context of targeting an intracellular reporter gene or endogenous gene.

EXPERIMENTAL SECTION

Materials

DNA oligonucleotides were purchased from Integrated DNA Technologies (www.idtdna.com) and used without further purification. t-Boc protected peptide nucleic acid monomers were purchased from Applied Biosystems and used for standard solid phase synthesis of the PNA oligomers.[28] (PNA monomers are no longer sold by this company. Presently they can be purchased from ASM Research Chemicals; Hannover, Germany, or synthesized in-house). The PNA oligomers were purified by reverse phase HPLC and verified by MALDI-TOF mass spectrometry (Applied Biosystems, Voyager DE sSTR) using sinapinic acid as the matrix $P_{myc}H$: expected m/z, 2460.2; found, 2462.52. $P_{telo}H$: expected 2701.47; found, 2703.28; $P_{myc}C$: expected m/z, 2181.3; found, 2179.1 $P_{telo}C$: expected 2471; found, 2470.7.

All DNA and PNA concentrations were determined by measuring the absorbance at 260 nm at 85°C on a Cary 3 Bio spectrophotometer. At high temperatures the bases are assumed to be unstacked and the extinction coefficient of the oligomer is estimated as the sum of the individual bases. For the DNA oligomers the extinction coefficients were used as reported in literature.[29] The PNA extinction coefficients at 260nm were obtained from Applied Biosystems. (A: 13700 $M^{-1}cm^{-1}$; C: 6600 $M^{-1}cm^{-1}$; G: 11700 $M^{-1}cm^{-1}$ and T: 8600 $M^{-1}cm^{-1}$). The cyanine dye $DiSC_2(5)$ was purchased from Molecular Probes, Inc. (Eugene, OR) and used without further purification. Stock solutions were prepared in methanol, and concentrations were determined using the manufacturer's extinction coefficient (ε_{651} = 260,000 $M^{-1}cm^{-1}$). $DiSC_1(3)$ was synthesized by Dr. Gloria Silva. Product was characterized using ESI mass spectrometry (Thermo-Fischer LCQ ESI/APCI Ion Trap). ($DiSC_1(3)$, expected m/z for M^+, 337.4; found, 337.3). UV-vis spectra for the compound matched the literature.[30]

Equipment

UV-vis measurements were performed on a Varian Cary 3 spectrophotometer equipped with a thermoelectrically controlled multicell holder. Circular dichroism (CD) spectra were recorded on a Jasco J-715 spectropolarimeter equipped with a thermoelectrically controlled single cell holder.

Surface plasmon resonance (SPR)

SPR measurements were performed by using a BIACore 2000 system with streptavidin-coated sensor chips (SA) for all experiments. DNA was immobilized on the surface by noncovalent capture to streptavidin. To prepare sensor chips for use, they were conditioned with five consecutive 1-min injections of 1 M NaCl in 50 mM NaOH followed by extensive washing with HEPES buffer, pH 7.4 [0.01 M HEPES, 0.15 M LiCl, 3 mM EDTA, and 50 μl/liter Surfactant P20]. 5′-Biotinylated oligonucleotide (25nM) in coupling buffer (10 mM HEPES, pH 7.4, 3 mM EDTA, and 150 mM LiCl) was heated at 95 °C for 5 min and cooled slowly to room temperature, and then injected at a flow rate of 2 μL/min to achieve long contact times with the surface and to control the amount of the DNA immobilized. Approximately 420 response units (RUs) of either Myc19 or hTelo22 were immobilized on separate flow cells. This is approximately 4-fold higher surface density than we used previously for SPR analysis of PNA-DNA hybridization and provided improved signal-to-noise ratios at lower PNA concentrations without altering the observed kinetics (Figure S3).

Direct binding experiments involved flowing homologous or complementary PNA over the chip surface as described previously.[16c]

Circular Dichroism Spectropolarimetry

CD measurements were performed on a Jasco J-715 CD spectropolarimeter equipped with water circulating temperature controller. Samples were prepared by mixing 1 μM DNA and 2 μM PNA together in 10 mM Tris-HCl (pH 7), 0.1mM EDTA and 100 mM Salt. Samples were annealed by heating to 95°C for five minutes and then slowly cooling to room temperature. All spectra were collected at 37°C by equilibrating the solutions at this temperature for 10min prior to recording. Each spectrum represents an average of 6 scans, collected at a rate of 100 nm min^{-1}. The spectra were baseline corrected. For recording the induced CD spectra of $DiSC_2(5)$, 10 μM of $DiSC_2(5)$ dye was added into pre-annealed mixture of 2 μM DNA and 4 μM PNA. The spectra were recorded at 25°C by equilibrating the solutions at this temperature for 10 min prior to recording. Each spectrum represents an average of 2 scans, collected at a rate of 200 nm min^{-1}. The spectra were baseline corrected.

Absorption spectroscopy

Mixtures of DNA and 2 equivalents of PNA were annealed by heating to 95°C for 5 min and then slowly cooling to room temperature. The dye ($DiSC_2(5)$ or $DiSC_1(3)$) was added to the samples and allowed to equilibrate at room temperature for 5 minutes after which the absorption spectra were collected using Varian Cary 300 Bio UV-Visible Spectrophotometer. Corresponding baseline corrections were made prior to absorbance measurement.

Emission spectroscopy

Emission (fluorescence) spectra of pre-annealed samples were collected using a Varian Cary Eclipse Fluorescence Spectrophotometer. Samples containing DNA, PNA and $DiSC_1(3)$ dye were prepared in a buffer solution containing 10 mM Tris-HCl (pH 7), 0.1 mM EDTA and 100 mM salt.

For determining PNA-DNA stoichiometries, continuous variation experiments were performed in which PNA and DNA were mixed at varying ratios but constant total concentration of 1 μM. Dye was also present at 1 μM concentration. Fluorescence spectra were recorded with excitation at 520 nm and the fluorescence intensity at 580 nm was plotted versus the PNA mole fraction to determine the empirical stoichiometry of PNA-DNA complex.

Supplementary Material

Refer to Web version on PubMed Central for supplementary material.

Acknowledgments

The authors gratefully acknowledge generous support of this research from the U.S. National Institutes of Health (R01GM058547 to BAA and DHL and R01AI064200 to WDW) and from the David Scaife Family Charitable Foundation (BAA).

References

1. Bochman ML, Paeschke K, Zakian VA. Nature Rev Gen. 2012; 13:770–780.
2. Huppert J. FEBS J. 2010; 277:3452–3458. [PubMed: 20670279]
3. Williamson JR, Raghuraman MK, Cech TR. Cell. 1989; 59:871–880. [PubMed: 2590943]

4. a) Todd AK, Johnston M, Neidle S. Nucleic Acids Res. 2005; 33:2901–2907. [PubMed: 15914666] b) Todd AK, Neidle S. Nucleic Acids Res. 2011; 39:4917–4927. [PubMed: 21357607] c) Huppert JL, Balasubramanian S. Nucleic Acids Res. 2005; 33:2908–2916. [PubMed: 15914667] d) Huppert J, Balasubramanian S. Nucleic Acids Res. 2007; 35:406–413. [PubMed: 17169996] e) Eddy J, Vallur AC, Varma S, Liu H, Reinhold WC, Pommier Y, Maizels N. Nucleic Acids Res. 2011; 39:4975–4983. [PubMed: 21371997] f) Zhao Y, Du Z, Li N. FEBS Lett. 2007; 581:1951–1956. [PubMed: 17462634]
5. a) Balasubramanian S, Hurley LH, Neidle S. Nature Rev Drug Discov. 2011; 10:261–275. [PubMed: 21455236] b) Siddiqui-Jain A, Grand CL, Bearss DJ, Hurley LH. Proc Natl Acad Sci USA. 2002; 99:11593–11598. [PubMed: 12195017]
6. Fernando H, Sewitz S, Darot J, Tavaré S, Huppert JL, Balasubramanian S. Nucleic Acids Res. 2009; 37:6716–6722. [PubMed: 19745055]
7. Lipps HJ, Rhodes D. TRENDS in Cell Biology. 2009; 19:414–422. [PubMed: 19589679]
8. a) Sissi C, Gatto B, Palumbo M. Biochimie. 2011; 93:1219–1230. [PubMed: 21549174] b) González V, Hurley LH. Biochemistry. 2010; 49:9706–9714. [PubMed: 20932061]
9. a) Fernando H, Rodriguez R, Balasubramanian S. Biochemistry. 2008; 47:9365–9371. [PubMed: 18702511] b) Schaffitzel C, Postberg J, Paeschke K, Lipps HJ. Meth Mol Biol. 2010; 608:159–181.
10. Biffi G, Tannahill D, McCafferty J, Balasubramanian S. Nature Chem. 2013
11. Luedtke NW. Chimia. 2009; 63:134–139.
12. Panyutin IG, Onyshchenko MI, Englund EA, Appella DH, Neumann RR. Curr Pharm Des. 2012; 18:1984–1991. [PubMed: 22376112]
13. a) Datta B, Armitage BA. J Am Chem Soc. 2001; 123:9612–9619. [PubMed: 11572682] b) Green JJ, Ying L, Klenerman D, Balasubramanian S. J Am Chem Soc. 2003; 125:3763–3767. [PubMed: 12656607] c) Amato J, Oliviero G, De Pauw E, Gabelica V. Biopolymers. 2009; 91:244–255. [PubMed: 19065573]
14. Amato J, Pagano B, Borbone N, Oliviero G, Gabelica V, De Pauw E, D'Errico S, Piccialli V, Varra M, Giancola C, Piccialli G, Mayol L. Bioconjugate Chem. 2011; 22:654–663.
15. Datta B, Schmitt C, Armitage BA. J Am Chem Soc. 2003; 125:4111–4118. [PubMed: 12670232]
16. a) Roy S, Zanotti KJ, Murphy CT, Tanious FA, Wilson WD, Ly DH, Armitage BA. Chem Commun. 2011; 47:8524–8526.b) Lusvarghi S, Murphy CT, Roy S, Tanious FA, Sacui I, Wilson WD, Ly DH, Armitage BA. J Am Chem Soc. 2009; 131:18415–18424. [PubMed: 19947597] c) Roy S, Tanious F, Wilson WD, Ly DH, Armitage BA. Biochemistry. 2007; 46:10433–10443. [PubMed: 17718513]
17. Paul A, Sengupta P, Krishnan Y, Ladame S. Chem Eur J. 2008; 14:8682–8689. [PubMed: 18668497]
18. a) Ambrus A, Chen D, Dai J, Jones RA, Yang D. Biochemistry. 2005; 44:2048–2058. [PubMed: 15697230] b) Phan AT, Modi YS, Patel DJ. J Am Chem Soc. 2004; 126:8710–8716. [PubMed: 15250723]
19. Egholm M, Buchardt O, Christensen L, Behrens C, Freier SM, Driver DA, Berg RH, Kim SK, Nordén B, Nielsen PE. Nature. 1993; 365:566–568. [PubMed: 7692304]
20. Seenisamy J, Rezler EM, Powell TJ, Tye D, Gokhale V, Joshi CS, Siddiqui-Jain A, Hurley LH. J Am Chem Soc. 2004; 126:8702–8709. [PubMed: 15250722]
21. Smith JO, Olson DA, Armitage BA. J Am Chem Soc. 1999; 121:2686–2695.
22. Mohammed HS, Delos Santos JO, Armitage BA. Artif DNA PNA XNA. 2011; 2:43–49. [PubMed: 21912726]
23. Ambrus A, Chen D, Dai J, Bialis T, Jones RA, Yang D. Nucleic Acids Res. 2006; 34:2723–2735. [PubMed: 16714449]
24. a) Marin VL, Armitage BA. J Am Chem Soc. 2005; 127:8032–8033. [PubMed: 15926825] b) Marin VL, Armitage BA. Biochemistry. 2006; 45:1745–1754. [PubMed: 16460021]
25. Arora R, Brun CMC, Azzalin CM. Prog Mol Subcell Biol. 2011; 51:65–94. [PubMed: 21287134]
26. Ito K, Go S, Komiyama M, Xu Y. J Am Chem Soc. 2011; 133:19153–19159. [PubMed: 22007660]
27. a) Thomas SM, Sahu B, Rapireddy S, Bahal R, Wheeler SE, Procopio EM, Joyce SC, Contrucci S, Wang Y, Chiosea SI, Lathrop KL, Watkins S, Grandis JR, Armitage BA, Ly DH. ACS Chemical

Biology. 2013; 8:345–352. [PubMed: 23113581] b) Hu J, Corey DR. Biochemistry. 2007; 46:7581–7589. [PubMed: 17536840] c) Shiraishi T, Nielsen PE. Bioconjugate Chem. 2012; 23:196–202.

28. a) Christensen L, Fitzpatrick R, Gildea B, Petersen KH, Hansen HF, Koch T, Egholm M, Buchardt O, Nielsen PE, Coull J, Berg RH. J Pept Sci. 1995; 3:175–183. [PubMed: 9222994] b) Koch, T. Peptide Nucleic Acids: Protocols and Applications. 2. Nielsen, PE., editor. Horizon Bioscience; Norfolk: 2004. p. 37-60.
29. Dawson, RMC.; Elliott, DC.; Elliott, WH.; Jones, KM. Data for Biochemical Research. Oxford University Press; New York: 1986. p. 103-114.
30. Yarmoluk SM, Kovalska VB, Lukashov SS, Slominskii YL. Bioorg Med Chem Lett. 1999; 9:1677–1678. [PubMed: 10397499]

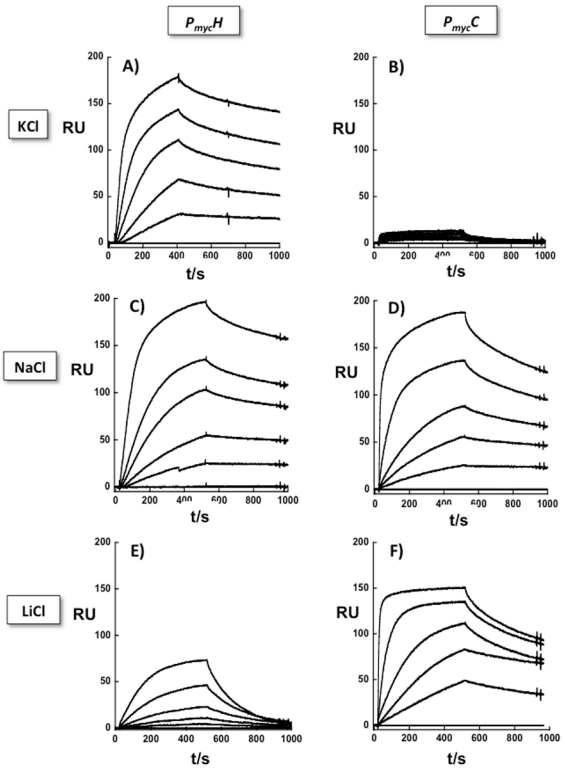

Figure 1.

SPR sensorgrams for binding of $P_{myc}H$ (left panels) or $P_{myc}C$ (right panels) to immobilized Myc19 in the presence of 100 mM KCl (A and B), NaCl (C and D) or LiCl (E and F). [PNA] = 0, 5, 10, 20, 40 and 80 nM.

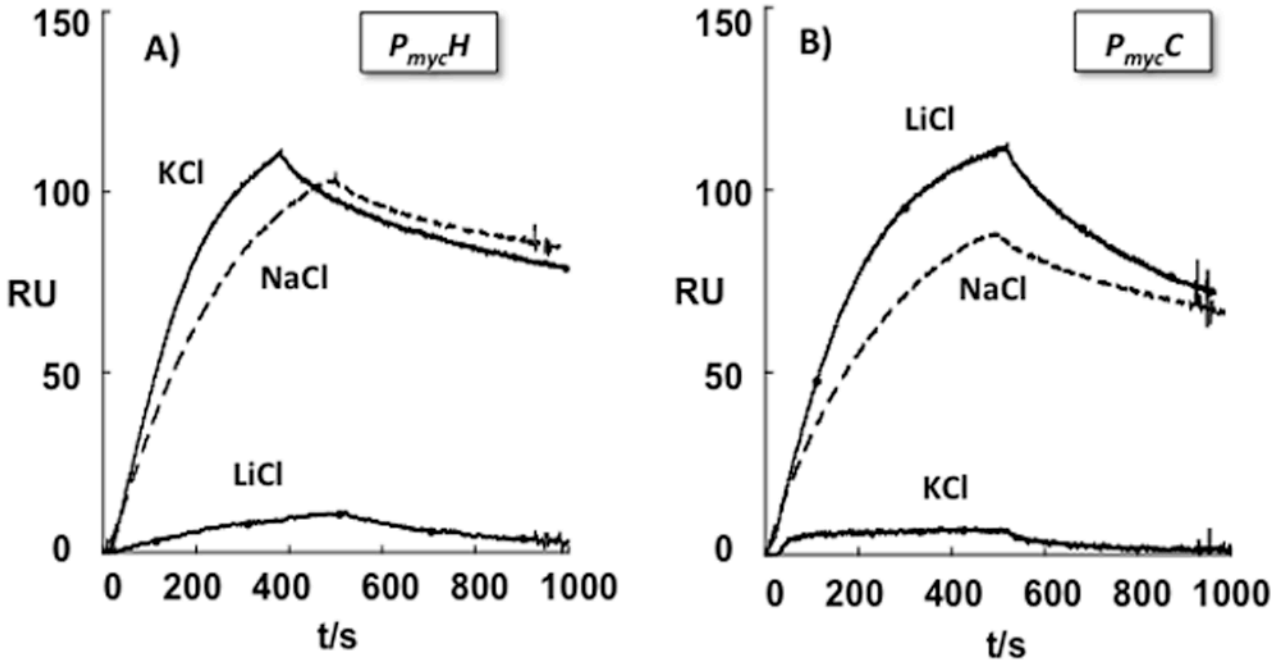

Figure 2.
Overlay of SPR sensorgrams recorded for binding of 20 nM $P_{myc}H$ (left) or $P_{myc}C$ (right) to immobilized Myc19 in 100 mM KCl, NaCl or LiCl.

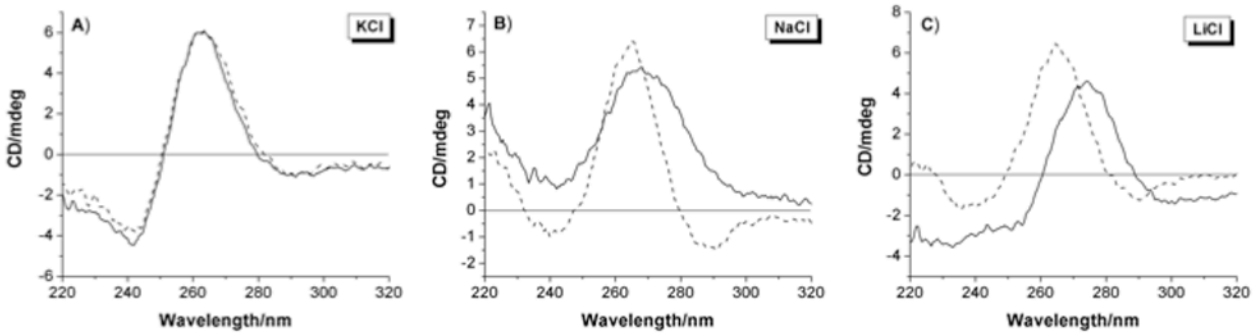

Figure 3.
CD spectra for 2 μM Myc19 quadruplex alone (solid lines) or with 4 μM $P_{myc}C$ (dashed lines). Samples contained 100 mM KCl (A), NaCl (B) or LiCl (C).

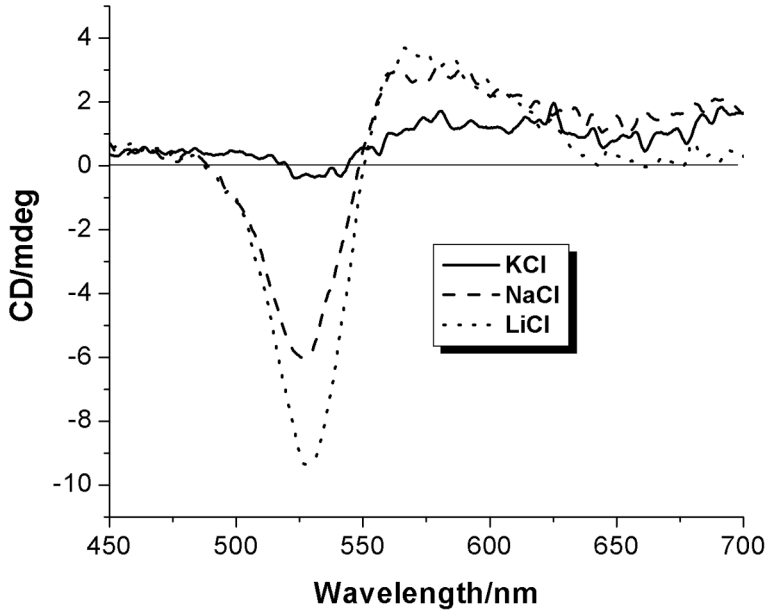

Figure 4.

Induced CD spectra of 10 μM $DiSC_2(5)$ in the presence of a 1:2 mixture of Myc19 DNA (2 μM) and $P_{myc}C$ PNA (4 μM) in 100 mM salt.

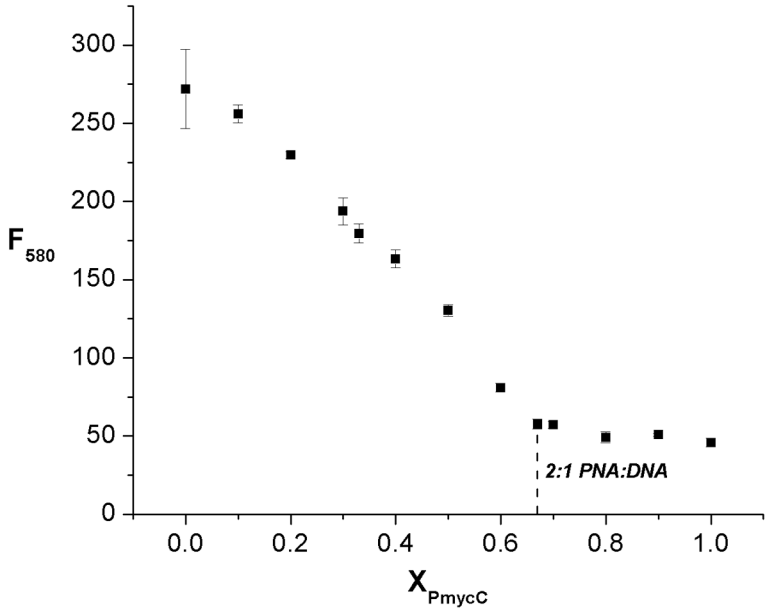

Figure 5.
Fluorescence of $DiSC_1(3)$ at 580 nm in Myc19:$P_{myc}C$ solutions of varying mole fraction of PNA. [Dye] = 1 μM, [NaCl] = 100 mM.

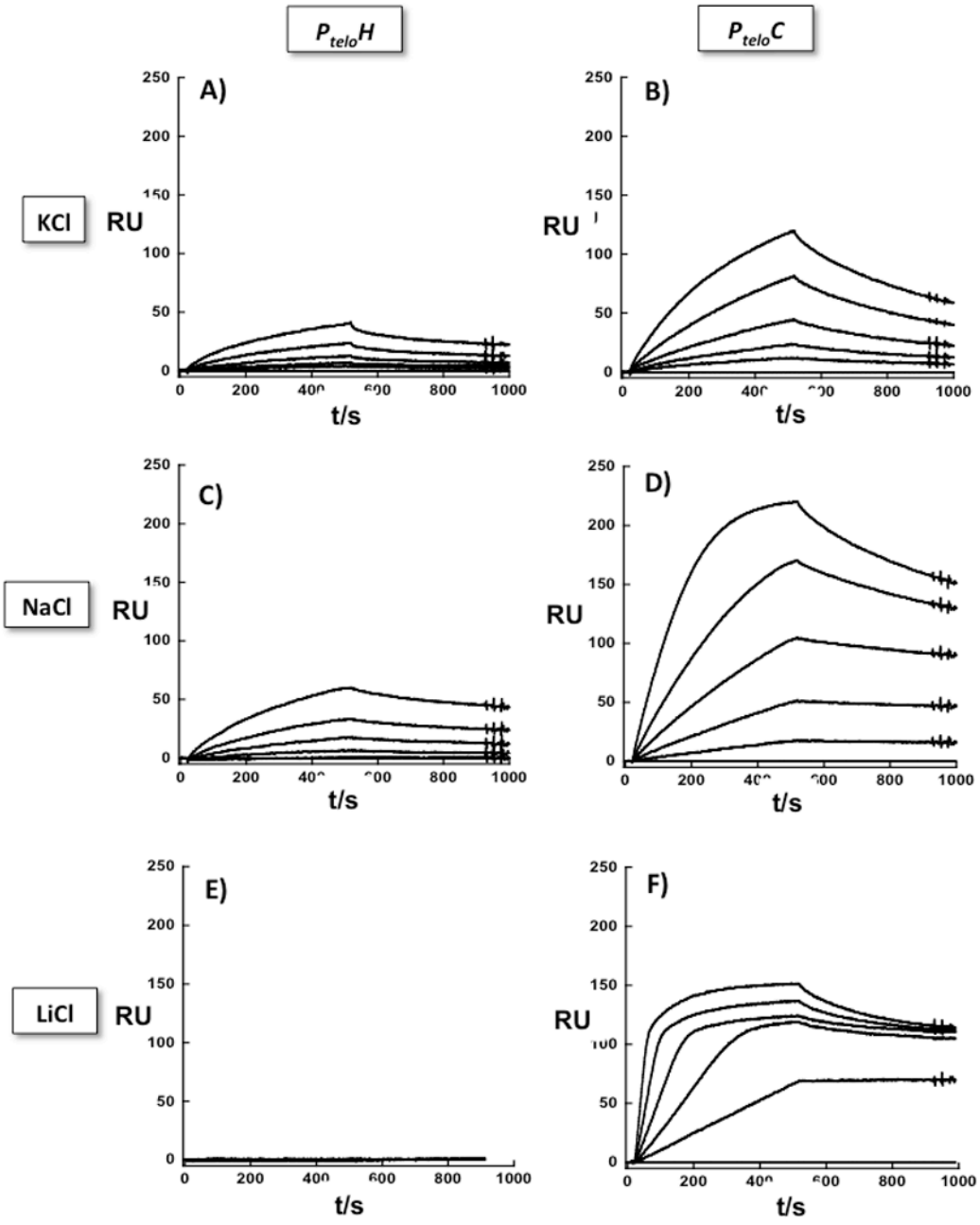

Figure 6.

SPR sensorgrams for binding of $P_{telo}H$ (left panels) or $P_{telo}C$ (right panels) to immobilized hTelo22 in the presence of 100 mM KCl (A and B), NaCl (C and D) or LiCl (E and F). [PNA] = 0, 5, 10, 20, 40 and 80 nM.

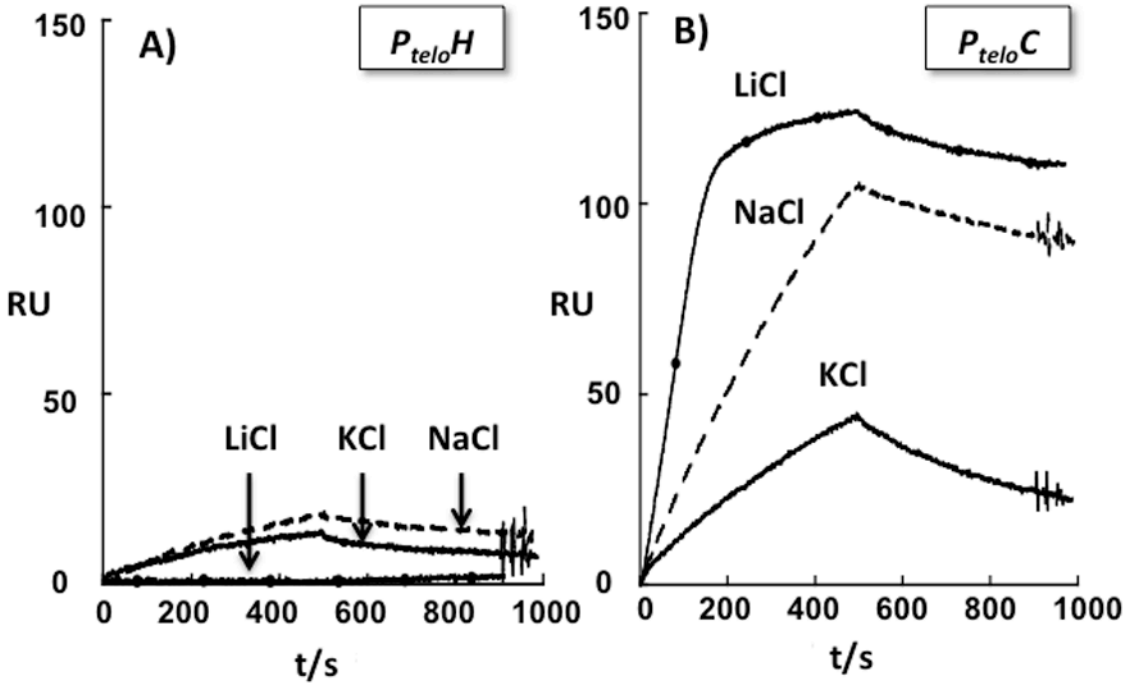

Figure 7.
Overlay of SPR sensorgrams recorded for binding of 20 nM $P_{telo}H$ (A) or $P_{telo}C$ (B) to immobilized hTelo22 in 100 mM KCl, NaCl or LiCl.

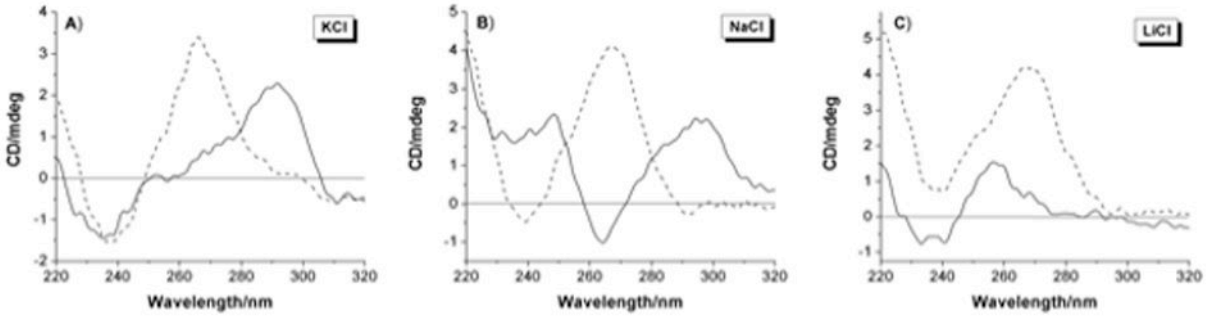

Figure 8.
CD spectra for 2 μM hTelo22 quadruplex alone (solid lines) or with 4 μM $P_{telo}C$ (dashed lines). Samples contained 100 mM KCl (A), NaCl (B) or LiCl (C).

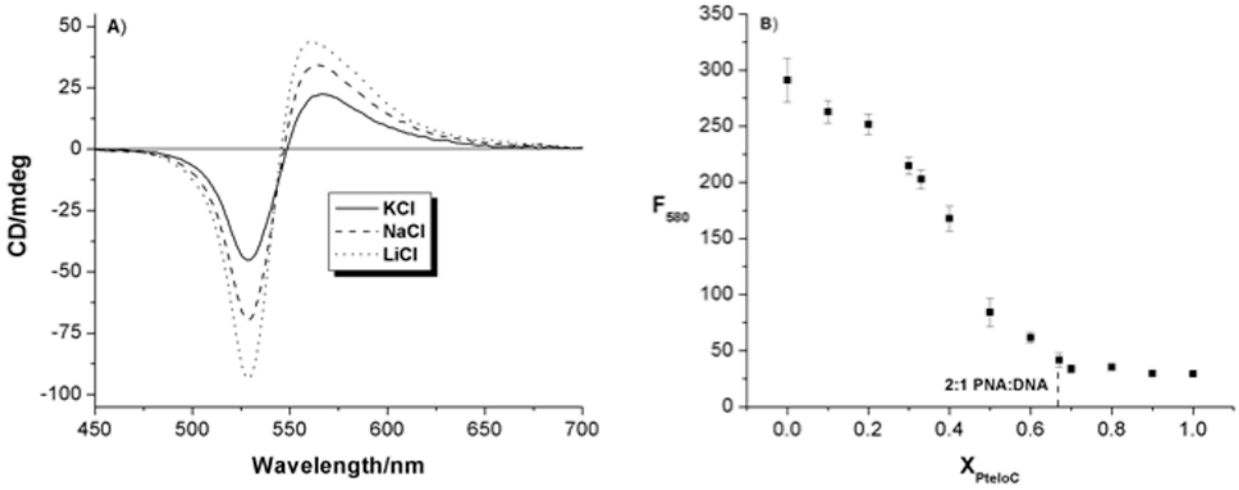

Figure 9.

(A) Induced CD spectra for 10 μM $DiSC_2(5)$ in the presence of 2:1 $P_{telo}C$:hTelo22 and KCl, NaCl or LiCl. (B) Job plot determined for $P_{telo}C$:hTelo22 using 1 μM $DiSC_1(3)$ in the presence of 100 mM LiCl.

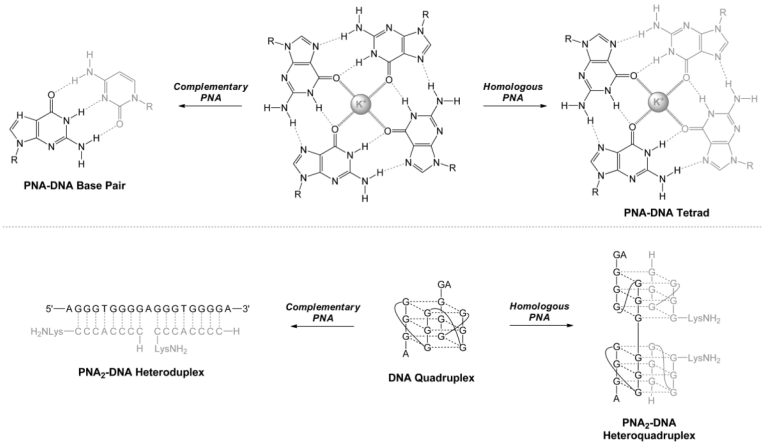

Scheme 1.

Top: Disruption of a DNA G-tetrad by complementary or homologous PNA results in Watson-Crick G-C pair or hetero-G-tetrad formation, respectively. *Bottom:* Proposed structures of PNA_2-DNA heteroduplex and heteroquadruplex formed by Myc19 DNA and complementary or homologous PNA.

Table 1

PNA probes, DNA quadruplex targets and cyanine dye structures

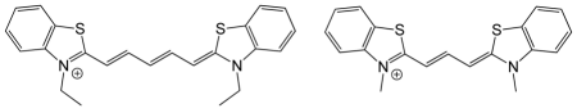

$DiSC_2(5)$

$DiSC_1(3)$

PNA	Sequence[†]
$P_{myc}H$	H-GGGGAGGG-$LysNH_2$
$P_{myc}C$	H-CCCCACCC-$LysNH_2$
$P_{telo}H$	H-GGGTTAGGG-$LysNH_2$
$P_{telo}C$	H-CCCTAACCC-$LysNH_2$

DNA	Sequence[‡]
Myc19	5′-AGGGTGGGGAGGGTGGGGA-3′
hTelo22	5′-AGGGTTAGGGTTAGGGTTAGGG-3′

[†]PNA sequences are written N-to-C; C-terminus is a lysine amide.

[‡]Guanines involved in G-tetrad formation are underlined.